**University of Bath**

**Alternative formats**
If you require this document in an alternative format, please contact:
openaccess@bath.ac.uk

# Experimental and Computational Studies of Ruthenium Complexes Bearing *Z*-Acceptor Aluminium-Based Phosphine Pincer Ligands

Connie J. Isaac, Cameron I. Wilson, Arron L. Burnage, Fedor M. Miloserdov, Mary F. Mahon, Stuart A. Macgregor[*] and Michael K. Whittlesey[*]

**Abstract:** Reaction of [Ru(C$_6$H$_4$PPh$_2$)$_2$(Ph$_2$PC$_6$H$_4$AlMe(THF))H] with CO results in clean conversion to the Ru–Al heterobimetallic complex [Ru(AlMePhos)(CO)$_3$] (**1**), where AlMePhos is the novel P–Al(Me)–P pincer ligand (*o*-Ph$_2$PC$_6$H$_4$)$_2$AlMe. Under photolytic conditions **1** reacts with H$_2$ to give [Ru(AlMePhos)(CO)$_2$H$_2$] (**2**) that is characterized by multinuclear NMR and IR spectroscopies. DFT calculations indicate that **2** features one terminal and one bridging hydride that are respectively *anti* and *syn* to the Al*Me* group. Calculations also define a mechanism for H$_2$ addition to **1** and predict facile hydride exchange in **2** that is also observed experimentally. Reaction of **1** with B(C$_6$F$_5$)$_3$ results in Me-abstraction to form the ion-pair [Ru(AlPhos)(CO)$_3$][MeB(C$_6$F$_5$)$_3$] (**4**) featuring a cationic [(*o*-Ph$_2$PC$_6$H$_4$)$_2$Al]$^+$ ligand, [AlPhos]$^+$. The Ru–Al distance in **4** (2.5334(16) Å) is significantly shorter than that in **1** (2.6578(6) Å), consistent with an enhanced Lewis acidity of the [AlPhos]$^+$ ligand. This is corroborated by a blue shift in both the observed and computed ν$_{CO}$ stretching frequencies upon Me abstraction. Electronic structure analyses (QTAIM, EDA-ETS) comparing **1**, **4** and the previously reported [Ru(ZnPhos)(CO)$_3$] analogue (ZnPhos = (*o*-Ph$_2$PC$_6$H$_4$)$_2$Zn) indicate the Lewis acidity of these pincer ligands increases along the series ZnPhos < AlMePhos < [AlPhos]$^+$.

**Introduction**

Sigma-accepting (or *Z*-type) ligands incorporating Lewis acidic $E(X)_n$ functionalities have become prominent in the last few years because of their ability to interact with transition metal (TM) centres to afford complexes with unusual coordination geometries and high reactivity.[1,2] One commonly used approach to stabilize $TM \rightarrow E(X)_n$ interactions involves the use of peripheral P donors to form pincer phosphine ligands $P-E(X)_n-P$.[3-6] As the archetypal Lewis acids, group 13 elements, and in particular B, have been the focus of considerable attention and a rich chemistry has developed for B(alkyl/aryl)-derived pincers.[7-9] In contrast, far fewer examples of P–Al(X)–P ligands are known, and these are largely restricted to X = halide derivatives.[10-14] In one early example, Bourissou and co-workers showed that attempts to generate $Cu \rightarrow (P-Al(Cl)-P)$ and $Au \rightarrow (P-Al(Cl)-P)$ complexes through coordination of (o-$^i$Pr$_2$PC$_6$H$_4$)$_2$AlCl to Cu(I) and Au(I) halide precursors instead resulted in halide migration from the coinage metal to Al to afford zwitterionic products as a result of the high Lewis acidity of the AlCl moiety.[10,11]

In a recent report, we described the serendipitous formation and trapping of the novel Zn-based *Z*-acceptor pincer ligand (o-Ph$_2$PC$_6$H$_4$)$_2$Zn (abbreviated to ZnPhos) following reaction of the heterobimetallic ruthenium-zinc complex [Ru(PPh$_3$)(C$_6$H$_4$PPh$_2$)$_2$(ZnMe)$_2$] (**I**) with CO or an N-heterocyclic carbene (Scheme 1).[15,16] The precise steps leading to the formation of the ZnPhos ligand are not known, but the presence of two cyclometalated phosphine ligands able to couple onto the Lewis acidic Zn center appears to be one requirement. In accord with this, we now report the formation of the corresponding AlMePhos (= o-Ph$_2$PC$_6$H$_4$)$_2$AlMe; Scheme 2) ligand in the reaction of the bis-cyclometalated Ru−Al precursor, [Ru(C$_6$H$_4$PPh$_2$)$_2$(Ph$_2$PC$_6$H$_4$AlMe(THF))H] (**II**),[17] with CO. A combination of experimental and computational studies have been employed to probe the structure of the resulting AlMePhos complex, [Ru(AlMePhos)(CO)$_3$] (**1**), as well as its reactivity;

photochemical addition of $H_2$ at the Ru–Al bond and susceptibility to Lewis acid mediated AlMe-group abstraction to afford the cationic [P–Al–P]$^+$ complex, [Ru(AlPhos)(CO)$_3$][MeB(C$_6$F$_5$)$_3$] (**4**).
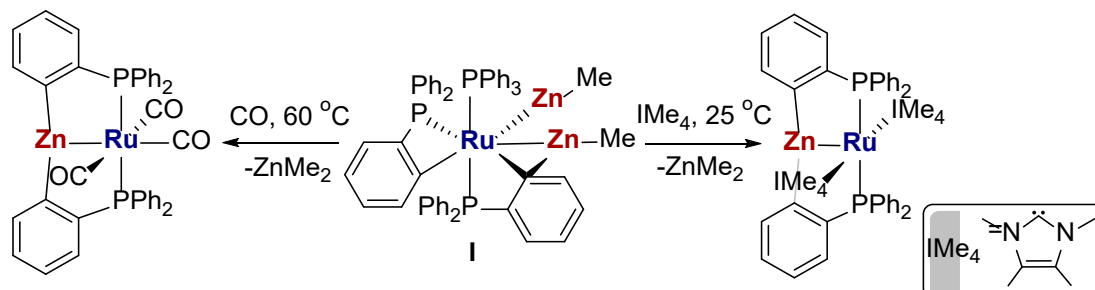


**Scheme 1.** Synthesis of [Ru(ZnPhos)] complexes from [Ru(PPh$_3$)(C$_6$H$_4$PPh$_2$)$_2$(ZnMe)$_2$] (**I**).

## Experimental

**General Comments**. All manipulations were carried out at room temperature under argon using standard Schlenk, high vacuum and glovebox techniques using dry and degassed solvents. C$_6$D$_6$ was vacuum transferred from potassium. NMR spectra were recorded in C$_6$D$_6$ at 298 K on Bruker Avance 400 and 500 MHz NMR spectrometers and referenced as follows: $^1$H, δ 7.15; $^{13}$C, δ 128.0. X{$^1$H} spectra were referenced externally to 85% H$_3$PO$_4$ (X = $^{31}$P), CFCl$_3$ (X = $^{19}$F) and BF$_3$·OEt$_2$ (X = $^{11}$B) at δ = 0. Coupling constants are defined using $^x J_{AB}$ nomenclature in cases where there is absolute certainty in assignments. IR spectra were recorded on Nicolet Nexus and Bruker ALPHA ATR-IR spectrometers. In-situ ReactIR monitoring of the conversion of **1** to **4** was carried out with a Mettler Toledo REACTIR15 system. Elemental analyses were performed by Elemental Microanalysis Ltd, Okehampton, Devon, U.K. [Ru(C$_6$H$_4$PPh$_2$)$_2${PPh$_2$C$_6$H$_4$AlMe(THF)}H] was prepared according to the literature.[17] B(C$_6$F$_5$)$_3$ (Alfa Aesar) was used as received.

**[Ru(AlMePhos)(CO)$_3$] (1)**. A C$_6$H$_6$ (6 mL) solution of [Ru(C$_6$H$_4$ PPh$_2$)$_2${PPh$_2$C$_6$H$_4$AlMe(THF)}H] (200 mg, 0.17 mmol) in a J. Youngs resealable ampule was

freeze-pump-thaw degassed (3 cycles), placed under 1 atm CO (or [13]CO to afford **1-[13]CO**) and heated at 60 °C for 2 h. The resulting yellow solution was filtered by cannula, concentrated (ca. 2 mL) and precipitated by addition of pentane to leave an off-white solid, that was recrystallized from benzene/hexane. Yield: 85 mg (67%) ^{1}H NMR (500 MHz, $C_6D_6$): δ 8.47 (d, $^3J_{HH}$ = 7.0 Hz, 2H, Ar), 7.77 (m, 4H, Ar), 7.36-7.30 (m, 6H, Ar), 7.20 (m, 2H, Ar), 7.04-6.97 (m, 8H, Ar), 6.90-6.85 (m, 6H, Ar), -0.24 (s, 3H, Al*Me*). ^{31}P{^{1}H} NMR (202 MHz, $C_6D_6$): δ 55.2 (s; **1-[13]CO**: m). ^{13}C{^{1}H} NMR (126 MHz, $C_6D_6$): δ 204.4 (t, $^2J_{CP}$ = 17 Hz, Ru-*C*O; **1-[13]CO**: dt, $^2J_{CC}$ = 27 Hz, $^2J_{CP}$ = 17 Hz), 202.0 (t, $^2J_{CP}$ = 13 Hz, Ru-*C*O; **1-[13]CO**: dt, $^2J_{CC}$ = 27 Hz, $^2J_{CP}$ = 13 Hz), 198.0 (t, $^2J_{CP}$ = 6 Hz, Ru-*C*O; **1-[13]CO**: br t, $^2J_{CP}$ = 5 Hz), 170.5 (vt, $J$ = 32 Hz, *i-C*-PAr), 142.7 (vt, $J$ = 32 Hz, *i-C*-PAr), 137.3 (vt, $J$ = 14 Hz, PAr), 137.0 (m, PAr), 133.6 (vt, $J$ = 6 Hz, PAr), 132.5 (vt, $J$ = 6 Hz, PAr), 131.4 (vt, $J$ = 5 Hz, PAr), 130.4 (s, PAr), 130.1 (s, PAr), 129.2 (s, PAr), 128.8 (vt, $J$ = 5 Hz, PAr), 128.5 (s, PAr), 128.4 (vt, $J$ = 4 Hz, PAr), 126.4 (vt, $J$ = 4 Hz, PAr), -5.0 (Al*Me* – observed by ^{1}H-^{13}C HSQC). IR: $v_{CO}$ ($C_6D_6$) = 2047, 1991, 1973 cm^{-1}; $v_{CO}$ (ATR) = 2042, 1989, 1961. Anal. Found: C, 65.43; H, 4.40. Calcd. For $C_{40}H_{31}O_3AlP_2Ru \cdot 0.5\ C_6H_6$: C, 65.48; H, 4.34.

**[Ru(AlMePhos)(CO)₂(μ−H)H] (2)**. A $C_6D_6$ (0.5 mL) solution of **1** (6 mg, 0.008 mmol) was freeze-pump-thaw degassed (3 cycles) in a J. Youngs resealable NMR tube and placed under 1 atm H₂. The tube was placed in a beaker of ice-cooled water and irradiated with a 500 W Hg arc lamp. Conversion to **2** (complete on this scale of reaction in ca. 3.5 h) was assessed by periodic removal of the sample from the lamp and NMR analysis. A larger scale reaction (20 mg of **1** in 1.5 mL $C_6H_6$ in a J. Youngs resealable ampule) was deemed to have reached maximum conversion (based upon NMR analysis) after ca. 13 h. Selected ^{1}H NMR (500 MHz, $C_6D_6$): δ 8.35 (d, $^3J_{HH}$ = 7.3 Hz, 2H, Ar), 7.65 (m, 5H, Ar), 7.45 (m, 4H, Ar), 7.28 (m, 4H, Ar), 6.95-6.90 (m, 3H, Ar),* -0.04 (s, 3H, Al*Me*), -6.18 (td, $^2J_{HP}$ = 20.2 Hz, $^2J_{HH}$ = 7.4 Hz, 1H, Ru-H), -8.56 (td, $^2J_{HP}$ = 16.4 Hz, $^2J_{HH}$ = 7.4 Hz, 1H, Ru-H-Al). [31]P{[1]H}

NMR (202 MHz, $C_6D_6$): δ 53.3 (s). Selected $^{13}C\{^1H\}$ NMR (100 MHz, $C_6D_6$): δ 198.5 (br m, Ru-$CO$). *Overlap of aromatic signals with those of [Ru(PPh$_3$)$_2$(CO)$_2$H$_2$] precluded full assignment of the aromatic $^1H$ NMR signals of **2**.

**[Ru(AlPhos)(CO)$_3$][MeB(C$_6$F$_5$)$_3$] (4).** Complex **1** (30 mg, 0.04 mmol) and B(C$_6$F$_5$)$_3$ (21 mg, 0.04 mmol) were added to a J. Youngs resealable NMR tube, dissolved in 0.5 mL $C_6D_6$ and full conversion into **4** observed by NMR spectroscopy over 2 h at room temperature. Cannula filtration, evaporation to dryness and redissolution in $C_6H_6$ followed by layering with pentane afforded colorless crystals of **4**. Yield: 22 mg (44%). $^1H$ NMR (500 MHz, $C_6D_6$): δ 8.26 (d, $^3J_{HH}$ = 7.0 Hz, 2H, Ar), 7.30 (t, $^3J_{HH}$ = 7.2 Hz, 2H, Ar), 7.22 (m, 7H, Ar), 7.12 (m, 1H, Ar), 7.00-6.84 (m, 16H, Ar), 1.58 (s, 3H, $Me$B(C$_6$F$_5$)$_3$). $^{31}P\{^1H\}$ NMR (202 MHz, $C_6D_6$): δ 52.3 (s). $^{13}C\{^1H\}$ NMR (126 MHz, $C_6D_6$): δ 197.6 (t, $^2J_{CP}$ = 13 Hz, Ru-$CO$), 194.8 (t, $^2J_{CP}$ = 6 Hz, Ru-$CO$), 160.2 (vt, $J$ = 26 Hz, PAr), 149.5 (br m, PAr), 147.6 (br m, PAr), 143.0 (vt, $J$ = 31 Hz, PAr), 137.0 (vt, $J$ = 12 Hz, PAr), 134.3 (vt, $J$ = 24 Hz, PAr), 133.0 (vt, $J$ = 6 Hz, PAr), 132.8 (vt, $J$ = 5 Hz, PAr), 132.4 (vt, $J$ = 6 Hz, PAr), 132.2 (vt, $J$ = 6 Hz, PAr), 131.4 (s, PAr), 131.0 (s, PAr), 129.2 (vt, $J$ = 6 Hz, PAr), 13.4 (B$Me$ – observed by $^1H$-$^{13}C$ HSQC). $^{11}B\{^1H\}$ NMR (160 MHz, $C_6D_6$): δ -14.7 (br s). $^{19}F\{^1H\}$ NMR (470 MHz, $C_6D_6$): δ -132.1 (br 's', 2F), -162.0 (br 's', 1F), -165.7 (br 's', 2F). IR: $\nu_{CO}$ ($C_6D_6$) = 2073, 2051 cm$^{-1}$. Anal. Found: C, 55.32; H, 2.52. Calcd. For C$_{58}$H$_{31}$BO$_3$F$_{15}$AlP$_2$Ru: C, 55.22; H, 2.48.

**X-ray crystallography.** Data for compounds **1** and **4** were collected on an Agilent SuperNova instrument using a Cu–Kα source. Both experiments were conducted at 150 K, solved using SHELXT[18,19] and refined using SHELXL[18] via the Olex2[20] interface. In the structure of **1**, the asymmetric unit plays host to one and a half molecules of benzene in addition to one molecule of the bimetallic complex. Both the organometallic molecule and the full-occupancy solvent entity are entirely ordered. However, the additional half benzene

moiety is disordered in a 50:50 ratio between two components. One of these lies close to a 2-fold crystallographic rotation axis and the other has two fractional occupancy carbons which are coincident with said symmetry element. Both ADP restraints and C–C distance restraints were included for fractional occupancy carbon atoms. The perfluorophenyl group based on C53, in the structure of **4**, was treated for 57:43 disorder. The rings of both components were refined as rigid hexagons. Additionally, both C–F and B–F distances (involving these fractional occupancy atoms) were refined subject to respective similarity restraints. The hydrogens attached to C4 were located and refined subject to being equidistant from the parent carbon.

**Computational Studies.** DFT calculations were run with Gaussian 09 (Revision D.01).[21] Geometry optimizations and thermodynamic corrections were performed with the BP86 functional[22,23] with Ru, Al and P centers described by Stuttgart RECPs and associated basis sets[24] and 6-31G** basis sets for all other atoms.[25,26] A set of d-orbital polarization functions was added to P ($\zeta^d = 0.387$).[27] All stationary points were fully characterized via analytical frequency calculations as either minima (all positive frequencies) or transition states (one negative frequency) and the latter were characterized via IRC calculations and subsequent geometry optimizations to confirm the adjacent minima. Electronic energies were recomputed with the ωB97x-D functional[28] using def2-TZVP basis sets[29,30] and a correction for benzene solvent (PCM approach).[31] This protocol was previously successful in reproducing the relative free energies of range of Ru-Zn heterobimetallic complexes in solution.[32] Details of all computed structures are provided in the Supporting Information. Quantum Theory of Atoms in Molecules (QTAIM) analyses[33] were performed with AIMALL[34] and used the extended wavefunction format. Extended Transition State-Energy Decomposition Analysis (ETS-EDA) calculations were run with the Amsterdam Modelling Suite AMS 2020.102.[35]

## Results and Discussion

**Synthesis of [Ru(AlMePhos)(CO)₃] (1) and reactivity with H₂.** Heating a benzene solution of [Ru(C₆H₄PPh₂)₂(Ph₂PC₆H₄AlMe(THF))H][17] under 1 atm CO for 2 h at 60 °C brought about clean conversion to [Ru(AlMePhos)(CO)₃] (**1**, Scheme 2), which was isolated as an off-white solid in 67% yield and fully characterized using a combination of NMR and IR spectroscopy (Figures S1-S7), X-ray crystallography (Figure 1) and elemental analysis. The $C_s$ symmetry imposed by the Al–Me group resulted in the appearance of three signals associated with the carbonyl groups in both the $^{13}C\{^1H\}$ NMR spectrum (δ 204, 202 and 198) and IR spectrum (2047, 1991 and 1973 cm$^{-1}$). The IR stretches are ca. 30-40 cm$^{-1}$ higher in frequency than those in [Ru(ZnPhos)(CO)₃], indicative of the Ru center being less electron-rich on account of the stronger $Z$-acceptor properties of the AlMePhos ligand. This was also borne out structurally, as evidenced by the lengthening of the Ru–$CO$ distance trans to E (E = AlMe, 1.971(2) Å; E = Zn, 1.951(3) Å). The Ru–Al distance of 2.6578(6) Å is within the sum of the covalent radii (2.67 Å)[36] indicative of a direct Ru–Al bond, and this is supported by the presence of a Ru–Al bond path in a QTAIM study (Figure S26). A more detailed discussion of the structure of **1** is provided below when comparing with the Me-abstracted [AlPhos]$^+$ complex **4**.
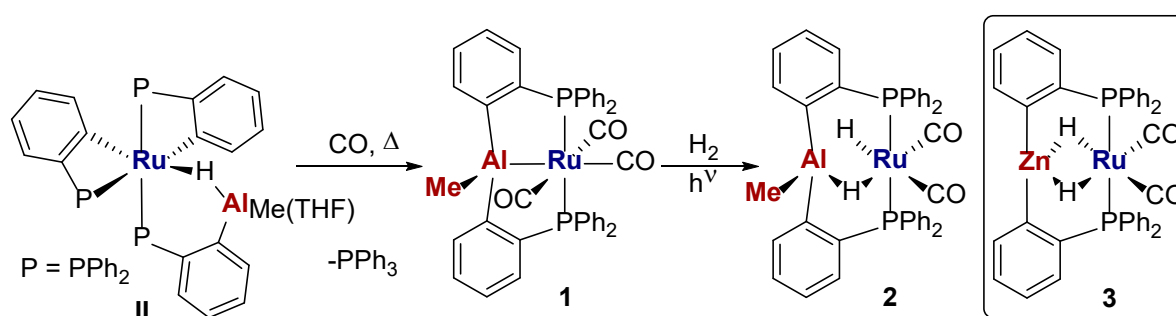


**Scheme 2.** Synthesis of [Ru(AlMePhos)(CO)₃] (**1**) and reaction with H₂ to give **2**. The structure of **2** is drawn on the basis of combined NMR and computational evidence discussed in the main text.

No thermal reaction of **1** in $C_6D_6$ with dihydrogen was observed (up to 60 °C), whereas UV photolysis under $H_2$ led to loss of the ^{31}P NMR resonance of the starting material at δ 55.2 and formation of a new singlet at δ 53.3, which was assigned to **2** (Scheme 2), the product of CO loss and subsequent $H_2$ addition. The ^{1}H NMR spectrum of **2** showed triplet of doublet hydride resonances at δ -6.18 and -8.56; these simplified to doublets with the same mutual $J_{HH}$ splitting (7.4 Hz) upon ^{31}P-decoupling (Figure S9), a measurement which revealed the slightly different linewidths (FWHM of 10.9 and 13.6 Hz respectively) of the two resonances (vide infra). We were unable to isolate **2** due to the co-formation of a second product, $[Ru(PPh_3)_2(CO)_2H_2]$ (Figures S9, S11-13),[37,38] which was also observed to form along with the ZnPhos photolysis product **3** (Scheme 2) and postulated to result from cleavage of the E–$C_6H_4$ (E = Zn, Al) bonds by adventitious moisture.[15] In support of this proposal, the concentration of the by-product varied between different experiments, showed no correlation with irradiation time (ruling out formation involving a secondary reaction with $H_2$)[39] and was (qualitatively) formed in greater amounts alongside **2** rather than **3**, which we attribute to the more polar/reactive Al–$C_6H_4$ bond.
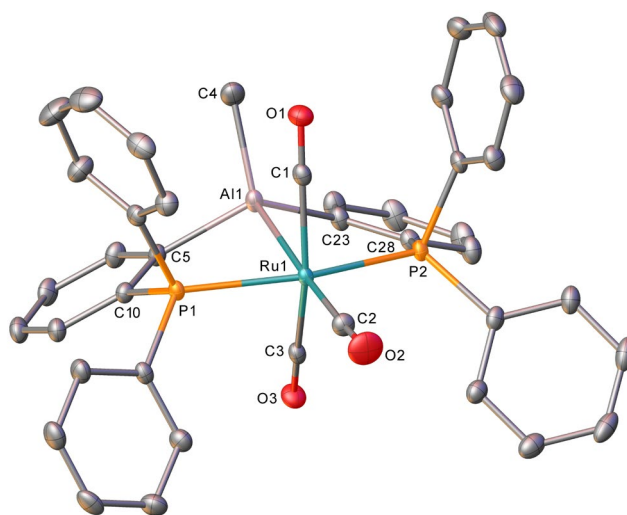


**Figure 1.** Molecular structure of **1**. Ellipsoids are represented at 30% probability. Hydrogen atoms and solvent have been omitted, for clarity.

Density functional theory (DFT) calculations were used to investigate both the structure and mechanism of formation of **2**. We assume that under photolytic conditions, loss of one CO ligand occurs to give 16e [Ru(AlMePhos)(CO)$_2$] (**1-CO**) for which several isomers are possible (Figure 2). CO loss trans to Al gives **_mer,trans_-1-CO**, the free energy of which is set to 0.0 kcal/mol. Loss of the cis CO ligands leads to either **_mer,cis_-1-CO**$_{cis}$ (+3.4 kcal/mol) or **_mer,cis_-1-CO**$_{trans}$ (+0.1 kcal/mol) depending on whether the Al–Me group is *syn* or *anti* to the vacant site. All three isomers show a distinct shortening of the Ru−Al distance (**1**: 2.74 Å (2.6578(6) Å experimentally); **_mer,trans_-1-CO**: 2.58 Å; **_mer,cis_-1-CO**$_{trans}$: 2.61 Å; **_mer,cis_-1-CO**$_{cis}$: 2.49 Å). The shorter Ru–Al distance in **_mer,cis_-1-CO**$_{cis}$ reflects a distortion of the Al–Me unit to engage in an agostic interaction involving one Me C–H bond (Ru···H = 2.28 Å; C–H = 1.12 Å). Distortion of the AlMePhos backbone is also seen in **_mer,cis_-1-CO**$_{trans}$ such that some degree of Ru···C(aryl) interaction is seen (Ru···C$_{aryl}$ = 2.60 Å). Both this and the agostic interaction in **_mer,cis_-1-CO**$_{cis}$ were corroborated by QTAIM studies (Figure S26). All three isomers can interconvert with barriers below 12 kcal/mol. As with the ZnPhos ligand, AlMePhos can also adopt a facial binding mode to give square-pyramidal geometries with either phosphorus (**_fac,cis_-1-CO**$_P$ : +11.0 kcal/mol) or Al (**_fac,cis_-1-CO**$_{Al}$: -3.6 kcal/mol) in the axial position. **_fac,cis_-1-CO**$_{Al}$ is therefore the most stable isomer of **1-CO**, however, the barrier for its formation via isomerization from the *mer*-isomers is 16 kcal/mol. As this is somewhat higher than the barriers for H$_2$ activation at the *mer*-isomers (vide infra), only the reactions of the latter with H$_2$ were considered. The greater stability of the *fac,cis*-isomer in the AlMePhos system reflects the ability of the {R$_2$AlMe} moiety to accommodate a pyramidal geometry at Al ($\Sigma_{angles}$ at Al = 338.7°), whereas the {R$_2$Zn} moiety in the equivalent isomer of [Ru(ZnPhos)(CO)$_2$] showed a distorted Zn center, with a C–Zn–C angle of 150.8°.[15]
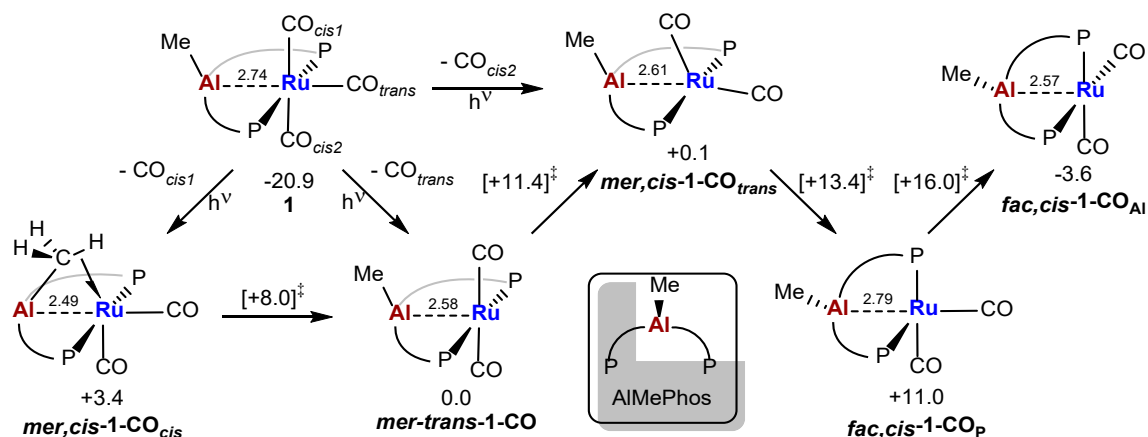
**Figure 2**. Computed isomers of [Ru(AlMePhos)(CO)$_2$] (**1-CO**) with free energies in kcal/mol. Isomerization transition state energies are shown in square brackets and Ru–Al distances in Å.

The addition of H$_2$ was modeled for all three *mer*-isomers of **1-CO** and the lowest energy pathway shown to start from ***mer,cis*-1-CO$_{trans}$** (Figure 3). H$_2$ addition proceeds with a barrier of 9.7 kcal/mol via **TS(1-2)1**, which exhibits a very early transition state geometry with long Ru···H distances (2.97 Å/3.07 Å) and minimal H–H bond elongation (0.75 Å). The distinct barrier arises from the need to distort the AlMePhos backbone to remove the short Ru···C$_{aryl}$ contact noted in the structure of ***mer,cis*-1-CO$_{trans}$** in order to make the vacant site at Ru available for H$_2$ addition. Beyond this transition state, H$_2$ cleavage proceeds without any subsequent barrier to give **Int(1-2)** at -7.0 kcal/mol. This intermediate exhibits one terminal Ru–hydride (Ru–H$_a$ = 1.65 Å) and a second hydride that bridges the Ru···Al vector (Ru–H$_b$ = 1.63 Å; Al–H$_b$ = 1.85 Å) with the Ru···Al distance increasing as a result to 2.87 Å. A facile rearrangement via **TS(1-2)2** at -4.1 kcal/mol moves H$_b$ across the Ru···Al vector to give **2** at -15.5 kcal/mol. The geometry of **2** again suggests one terminal hydride positioned anti to the Al–*Me* group (Ru–H$_a$ = 1.65 Å) and one bridging hydride syn to Al–*Me* (Ru–H$_b$ = 1.70 Å; Al–H$_b$ = 1.80 Å; Ru···Al = 2.94 Å) and this is supported by a QTAIM study that

10

showed the presence of the corresponding Ru–$H_a$, Ru–$H_b$ and Al–$H_b$ bond paths, but no

Al···$H_a$ bond path (Figure S26). The computational findings were consistent with

experimental observations on **2**; the presence of two hydride resonances, the slightly broader

nature of the lower frequency signal from bridging between Ru and quadrupolar Al, and $T_1$

values (400 MHz, 298 K) of 730 ms ($\delta$ -6.2) and 515 ms ($\delta$ -8.6), consistent with classical

hydrides.[40]

Of the other *mer*-isomers, $H_2$ activation at ***mer,cis*-1-CO*cis*** proceeds through a similar

pathway with a slightly higher barrier of 11.5 kcal/mol for the initial $H_2$ addition step. For

***mer,trans*-1-CO**, $H_2$ addition entails a smaller barrier of 4.3 kcal/mol to form an $\eta^2$-$H_2$

complex, ***mer-trans*-Int(1-2)1**, at -2.5 kcal/mol. This species can then isomerize to **2**,

however, this process has an overall barrier of 15.7 kcal/mol. $H_2$ addition to ***mer,trans*-1-CO**

will therefore be a reversible process, with isomerization to either of the *mer,cis*-isomers

providing access to the lower energy $H_2$ activation pathways associated with those species

(Figures S24 and S25).
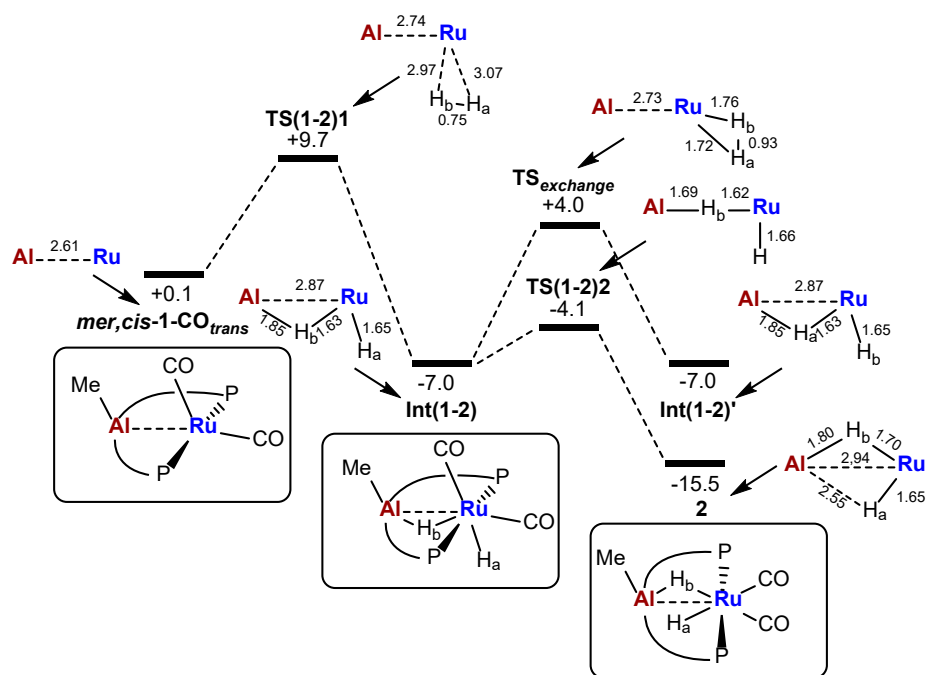
**Figure 3.** Computed reaction profile (kcal/mol) for the addition of $H_2$ to ***mer,cis*-1-CO***$_{trans}$** with key distances within the {$AlRuH_2$} moiety indicated in Å.

In general, the different isomers of **1-CO**, their interconversion and reactivity with $H_2$ all follow a similar pattern to that reported previously for their ZnPhos analogues.[15] However, the presence of the Al–*Me* group places the two hydrides in **2** in different environments ($H_a$: terminal; $H_b$: bridging) and hence offers the possibility of $H_a/H_b$ exchange. This was defined computationally from **2** by reverting back to **Int(1-2)** in which both $H_a$ and $H_b$ are on the same side of the Ru···Al vector (Figure 3). $H_a/H_b$ exchange then proceeds through **TS$_{exchange}$** at +4.0 kcal/mol that corresponds to the rotation of an $\eta^2$-$H_a$–$H_b$ moiety. The overall barrier for $H_a/H_b$ exchange is therefore predicted to be 19.5 kcal/mol. An alternative pathway involving inversion at the Al center was found to have a higher barrier of 33.8 kcal/mol. This low computed exchange barrier was verified experimentally by the appearance of an EXSY signal between the two hydrides, as well as a NOESY correlation from both hydrides to the Al–*Me* resonance (Figure S10).
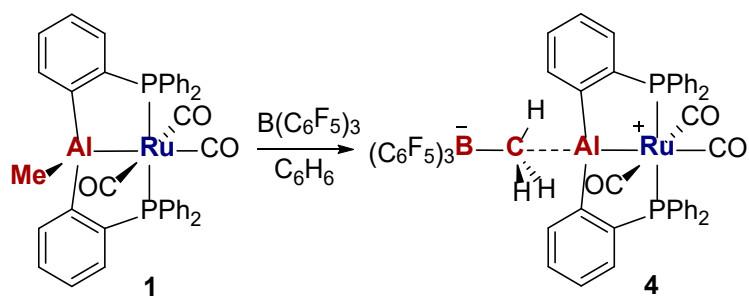
**Scheme 3.** Synthesis of [Ru(AlPhos)(CO)$_3$][MeB(C$_6$F$_5$)$_3$] (**4**).

**Complexation of [AlPhos]$^+$.** Treatment of **1** with an equimolar amount of B(C$_6$F$_5$)$_3$ in benzene resulted in abstraction of the Al−Me group and formation of the [MeB(C$_6$F$_5$)$_3$]$^-$ salt of the cationic aluminium pincer phosphine complex, [Ru(AlPhos)(CO)$_3$]$^+$ (**4**) (Scheme 3). The [MeB(C$_6$F$_5$)$_3$]$^-$ anion showed a characteristic downfield shift[41] of the methyl resonance in the $^1$H NMR spectrum from δ -0.24 in **1** to δ 1.50 in **4**. When the reaction was followed by ReactIR spectroscopy (Figure S23), loss of the carbonyl absorption bands for **1** at 2047, 1991 and 1973 cm$^{-1}$ was accompanied by growth of new bands for **4** at 2073 and 2051 cm$^{-1}$, the shift to higher frequency being consistent with the presence of the more Lewis acidic [AlPhos]$^+$ ligand.

Isolation of X-ray quality crystals yielded the structure of **4** shown in Figure 4. Particularly notable were the significant changes in the metrics relative to those in **1**; reduction of the Ru−Al distance (from 2.6578(6) Å to 2.5334(16) Å), elongation of the Ru−$C$O bond length trans to Al (from 1.971(2) Å to 1.986(6) Å) and shortening of the Al−$C_6$H$_4$ distances (from 2.0085 Å (average) to 1.979 Å (average)). In regard to the extent of interaction between the cation and anion, the Al···C and B–C distances of 2.354(7) and 1.684(10) Å respectively, and Al···C–B angle 171.5(5)°, are comparable to those found in [pySiMe$_2$(TMS)AlMe][MeB(C$_6$F$_5$)$_3$], which exhibits a crystallographically characterized Al···$Me$–B moiety.[42] In both cases the Al···C distance is well beyond the sum of the covalent

radii (1.97 Å)[36] although computational studies do suggest some residual interaction (see below). Near identical diffusion coefficients (Figure S21) for the cation and anion in this species, as well as a $\Delta^{19}F$ chemical shift difference of 3.7 ppm between the meta- and para-F resonances of the $[MeB(C_6F_5)_3]$ anion,[43,44] support ion pair character in solution; this is perhaps unsurprising given the established high Lewis acidity of $[AlR_2]^+$ cations.[45-47]
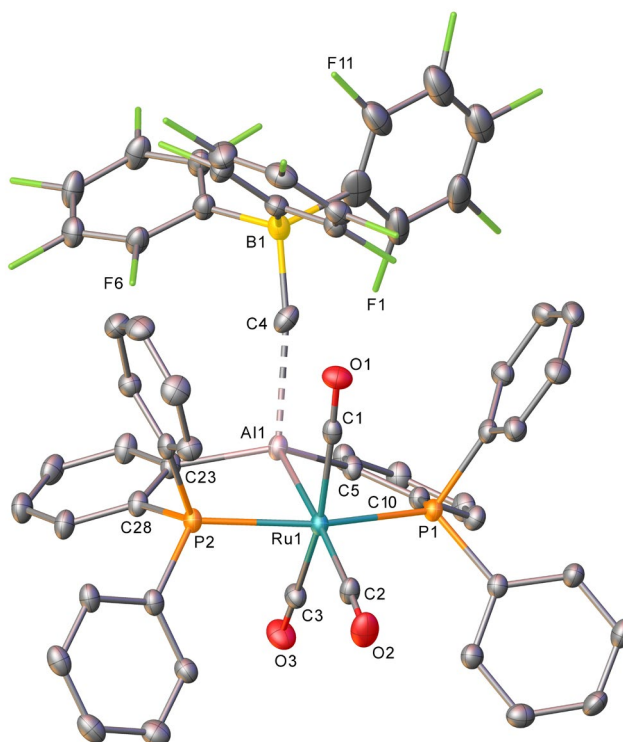


**Figure 4.** Molecular structures of **4**. Ellipsoids are represented at 30% probability. Hydrogen atoms, solvent and the minor components of disordered atoms have been omitted, for clarity.

Methyl group abstraction from **1** by $B(C_6F_5)_3$ was also modeled computationally and shown to proceed from a $\mathbf{1}\cdot B(C_6F_5)_3$ precursor adduct with a barrier of only 7.2 kcal/mol to form ion-pair **4** at -6.3 kcal/mol. The Me-abstraction transition state shows a near planar $CH_3$ unit ($\Sigma_{angles}$ at C = 356.9°) that is equidistant between the Al and B centers (Al···C = 2.15 Å; C···B = 2.15 Å). The Ru–Al distance also shortens to 2.67 Å enroute to its final computed value of 2.62 Å in **4**. As was the case for **1**, the computed Ru–Al distance in **4** is ca. 0.09 Å

longer than that determined experimentally, however the 0.12 Å shortening of the Ru–Al

distance upon Me-abstraction is nicely reproduced, as are the changes in Ru–$CO$ distances

between **1** and **4**.

Disappointingly, **4** exhibited only limited stability in solution, with redissolved

crystals of the compound decomposing in $C_6D_6$ over ca. 3 days to unknown products. We

postulate that this could involve reaction of the [MeB($C_6F_5$)$_3$]$^-$ anion, whose non-innocence is

well-established.[48]

**Electronic Structure Analyses of 1 and 4 and Comparison with**

**[Ru(ZnPhos)(CO)$_3$].** The nature of the Ru–Al interactions in **1** and **4** was probed through a

combination of QTAIM and ETS-EDA analyses. These were based on the experimental

structures with the heavy atoms fixed from the crystal structures and the H atoms optimized

with the BP86 functional. The QTAIM analysis of ion pair **4** reveals an Al···C(*Me*)–B bond

path with an electron density, $\rho(r)$, of 0.029 au at the bond critical point (BCP, Figure S26).

Moreover, optimisation of **4$^+$** (i.e. the cation in the absence of the [MeB($C_6F_5$)$_3$]$^-$ anion)

resulted in a shortening of the Ru–Al distance from 2.62 Å to 2.51 Å, and a widening of the

$C_{aryl}$–Al–$C_{aryl}$ angle from 127° to 138°. The presence of the anion therefore has some impact

on the structure of **4$^+$**, implying some degree of Al···C(*Me*) interaction is present.

BCP metrics for the Ru··Al bond paths in **1** and **4** are shown in Table 1 along with the

equivalent data for the Ru···Zn bond path in [Ru(ZnPhos)(CO)$_3$].[15] All three species show

low BCP $\rho(r)$ values that are typical of TM–E bonds of this type, while the small, negative

total energy densities, H(r), suggest a degree of covalent character.[49,50] The small ellipticities

of the Ru···Al bond paths are also indicative of cylindrical σ-interactions in both **1** and **4**,

despite the availability of a second vacant orbital in the latter (see the ETS-EDA analysis

below). Overall, all the BCP metrics indicate the Ru···Al interaction in **4** is somewhat

stronger than in **1**. Comparison of the Ru···Al interaction in **1** with the Ru···Zn interaction in

[Ru(ZnPhos)(CO)$_3$] is less clear-cut, as the main indicators of the strength of interaction, $\rho(r)$

and H(r), are contradictory (the former being smaller and the latter larger in **1**).

**Table 1.** Selected BCP metrics (in atomic units) for the Ru···Al bond paths in **1** and **4** and the

Ru···Zn bond path in [Ru(ZnPhos)(CO)$_3$].

| Species | Bond Path | $\rho(r)$ | $\nabla^2\rho(r)$ | $\varepsilon$ | H(r) |
|---|---|---|---|---|---|
| **1** | Ru···Al | 0.040 | +0.052 | 0.045 | -0.017 |
| **4** | Ru···Al | 0.051 | +0.061 | 0.029 | -0.024 |
| [Ru(ZnPhos)(CO)$_3$] | Ru···Zn | 0.045 | +0.039 | 0.035 | -0.014 |

The ETS-EDA analysis was performed on **1** and the **4**$^+$ cation and inspection of the

molecular orbitals of this species revealed the presence of one high-lying occupied orbital

with strong Ru–Al bonding character (Figure 5 for **4**$^+$). The nature of this interaction was

quantified within the ETS-EDA scheme by considering donation from the HOMO of the

common d$^8$ {Ru(CO)$_3$} fragment (Ru$^{HOMO}$, shown schematically in Figure 5) into the Al-

based LUMOs on the {AlMePhos} and {AlPhos}$^+$ fragments. Of these Al$^{LUMO1}$ is present in

both fragments, whereas Al$^{LUMO2}$ is only available in {AlPhos}$^+$. A similar analysis was also

performed for [Ru(ZnPhos)(CO)$_3$] and the key data are collected in Table 2.
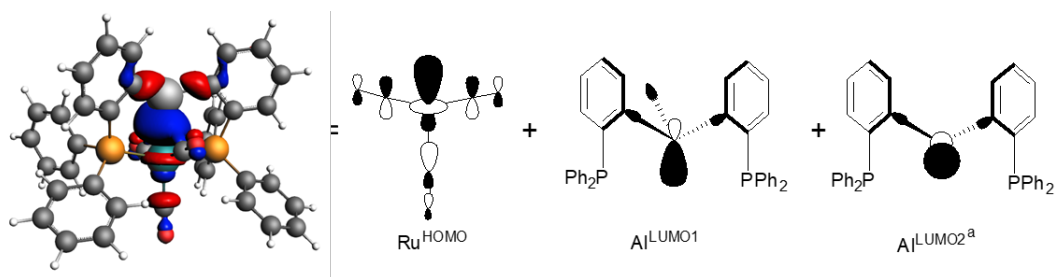
**Figure 5.** The Ru–Al bonding orbital in **4⁺** (HOMO-1) and schematics of the key fragment orbitals used in the ETS-EDA calculations on **1** and **4⁺**; [a]Al$^{LUMO2}$ is only present in **4⁺**.

Table 2 shows that for **1**, Ru$^{HOMO}$ is depopulated to 1.46e, with 0.32e being donated into Al$^{LUMO1}$. Upon Me abstraction to form **4⁺**, the population of Ru$^{HOMO}$ decreases further to 1.19e, reflecting the availability of a second acceptor orbital and a more Lewis-acidic [AlPhos]⁺ ligand, the two acceptor orbitals of which have a combined occupation of 0.58e. This is also reflected in an increase in the total interaction energy, $\Delta E^{Total}$, and its orbital interaction component, $\Delta E^{orbital}$. As the other three occupied Ru-based $d\pi$ orbitals in the {Ru(CO)₃} fragment showed essentially no variation in occupancy between **1** and **4⁺** (Figure S27), the stronger Ru–Al interaction in **4⁺** must arise from the stronger $\sigma$-acceptor properties of the [AlPhos]⁺ ligand rather than any $\pi$-acceptor character. This is also consistent with the low ellipticity noted in the QTAIM study. Comparing the ETS-EDA analyses of **1** and [Ru(ZnPhos)(CO)₃] shows the AlMePhos ligand causes a higher depopulation of Ru$^{HOMO}$ and provides greater values of $\Delta E^{Total}$ and $\Delta E^{orbital}$. The computed trend in ligand Lewis acidity is therefore [AlPhos]⁺ > AlMePhos > ZnPhos. This is also supported by the calculated CO stretching frequencies that show an increase of 20-30 cm⁻¹ from [Ru(ZnPhos)(CO)₃] to **1** and again from **1** to **4⁺**.

**Table 2.** ETS-EDA data for Ru–Al bonding in **1** and **4** and Ru–Zn bonding in **3**[a]

| Species | Orbital Populations | | | $\Delta E^{orbital}$ | $\Delta E^{Total\ a}$ | $\nu_{CO}$ (calc)/cm$^{-1}$ |
|---|---|---|---|---|---|---|
| | Ru$^{HOMO}$ | Al$^{LUMO1}$ | Al$^{LUMO2}$ | | | |
| **1** | 1.46 | 0.32 | | -234.2 | -169.7 | 2013, 1964, 1953 |
| **4**[b] | 1.19 | 0.21 | 0.37[c] | -282.9 | -193.2 | 2045, 1991, 1972 |
| [Ru(ZnPhos)(CO)₃] | 1.51 | 0.12[d] | | -215.7 | -156.1 | 1982, 1942, 1922 |

[a] $\Delta E^{Total}$ is the computed binding energy (kcal/mol) between the {Ru(CO)₃} fragment and the {AlMePhos}, {AlPhos}$^+$ and {ZnPhos} fragments in **1**, **4**$^+$ and [Ru(ZnPhos)(CO)₃] respectively. This is the sum of $\Delta E^{steric}$ (not shown) and $\Delta E^{orbital}$, the orbital interaction:[33] the magnitude of $\Delta E^{orbital}$ reflects the additional contributions from phosphine arms of the {AlMePhos} and {AlPhos}$^+$ fragments. [b] For the purposes of the ETS-EDA analysis, the **4**$^+$ cation was computed in the absence of the anion. [c] Al$^{LUMO2}$ is only present in {AlPhos}$^+$. [d] Occupation of the primary Zn-based acceptor orbital; several other acceptor orbitals with Zn character are also populated to some extent but are heavily delocalized over the ZnPhos ligand, meaning an accurate assessment of the total population at Zn is not possible.

## Conclusions

The synthesis and characterisation of the Ru–Al heterobimetallic complex [Ru(AlMePhos)(CO)₃] (**1**) has been presented, where AlMePhos is the novel P–Al(Me)–P pincer ligand (*o*-Ph₂PC₆H₄)₂AlMe. Under photolytic conditions **1** loses CO and activates H₂ to give [Ru(AlMePhos)(CO)₂(μ–H)H] (**2**), which has been characterized by multinuclear NMR and IR spectroscopies. DFT calculations define a low energy mechanism by which H₂ is activated at an unsaturated 16e Ru center before rearranging to form **2**, the most stable structure, which has one terminal and one bridging hydride that are respectively *anti* and *syn* to the Al*Me* group. The calculations predict facile hydride exchange on the NMR timescale, a process that was corroborated experimentally. Reaction of **1** with B(C₆F₅)₃ results in Me-abstraction to form the ion-pair [Ru(AlPhos)(CO)₃][MeB(C₆F₅)₃] (**4**) featuring the cationic [(*o*-Ph₂PC₆H₄)₂Al]$^+$ ligand, [AlPhos]$^+$. Crystallographic and computational characterization

suggest **4** exists as a close contact ion pair in the solid state with some Al⋯Me–B interaction; this ion-pairing is retained in benzene solution. Electronic structure analyses identify a Ru–Al bond in **1** that is strengthened upon Me abstraction to form **4**. Further electronic structure analyses comparing **1** and **4** with the previously reported [Ru(ZnPhos)(CO)$_3$] complex indicate the Lewis acidity of these pincer ligands increases along the series ZnPhos < AlMePhos < [AlPhos]$^+$. This is supported by the trends in both the experimental and computed $\nu_{CO}$ stretching frequencies. The AlMePhos and [AlPhos]$^+$ pincer ligands add to the growing family of main group analogues[4] of the widely used DPEPhos ligand, Ph$_2$P($o$-C$_6$H$_4$)$_2$O.[51]

## Associated Content

### Supporting Information

The supporting information is available free of charge at https://pubs.acs.org/doi/........... NMR and IR spectra of compounds **1**, **2** and **4**. Table S1. Structures and Cartesian coordinates (XYZ).

### Accession Codes

CCDC 2182238 and 2182239 for **1** and **4** contain the supplementary crystallographic data for this paper. These data can be obtained free of charge via www.ccdc.cam.ac.uk/data_request/cif, or by e-mailing data_request@ccdc.cam.ac.uk, or by contacting The Cambridge Crystallographic Database, 12 Union Road, Cambridge CB2 1EZ, UK.

## Author Information

### Corresponding Authors

**Stuart A. Macgregor** − Institute of Chemical Sciences, Heriot-Watt University, Edinburgh EH14 4AS, U.K.; orcid.org/ 0000-0003-3454-6776; E-mail: s.a.macgregor@hw.ac.uk

**Michael K. Whittlesey** − Department of Chemistry, University of Bath, Bath BA2 7AY, U.K.; orcid.org/0000-0002-5082-3203; E-mail: m.k.whittlesey@bath.ac.uk

**Authors**

**Connie J. Isaac** − Department of Chemistry, University of Bath, Bath BA2 7AY, U.K.

**Cameron I. Wilson** − Institute of Chemical Sciences, Heriot-Watt University, Edinburgh EH14 4AS, U.K.

**Arron L. Burnage** − Institute of Chemical Sciences, Heriot-Watt University, Edinburgh EH14 4AS, U.K.

**Fedor M. Miloserdov** − Department of Chemistry, University of Bath, Bath BA2 7AY, U.K. *Current address*: Laboratory of Organic Chemistry, Wageningen University, Stippeneng 4, Wageningen 6708 WE, The Netherlands; orcid.org/0000-0001-6420-211X.

**Mary F. Mahon** − Department of Chemistry, University of Bath, Bath, BA2 7AY, U.K.

**Notes**

The authors declare no competing financial interest.

**References**

(1)     Bouhadir, G.; Bourissou, D. Complexes of ambiphilic ligands: reactivity and catalytic applications. *Chem. Soc. Rev.* **2015**, *45*, 1065-1079.

(2)     You, D.; Gabbai, F. P. Tunable σ-accepting, Z-type ligands for organometallic catalysis. *Trends Chem.* **2019**, *1*, 485-496.

(3)     Bennett, M. A.; Bhargava, S. K.; Mirzadeh, N.; Privér. The use of [2-C$_6$R$_4$PPh$_2$]$^-$ (R = H, F) and related carbanions as building blocks in coordination chemistry. *Coord. Chem. Rev.* **2018**, *350*, 69-128.

(4)     Vogt, M.; Langer, R. The pincer platform beyond classical coordination patterns. *Eur. J. Inorg. Chem.* **2020**, 3885-3898.

(5)     Takaya, J. Catalysis using transition metal complexes featuring main group metal and metalloid compounds as supporting ligands. *Chem. Sci.* **2021**, *12*, 1964-1981.

(6)     Komuro, T.; Nakajima, Y.; Takaya, J.; Hashimoto, H. Recent progress in transition metal complexes supported by multidentate ligands featuring group 13 and 14 elements as coordinating atoms. *Coord. Chem. Rev.* **2022**, *473*, 214837.

(7)     Sircoglou, M.; Bontemps, S.; Mercy, M.; Miqueu, K.; Ladeira, S.; Saffon, N.; Maron, L.;  Bouhadir, G.; Bourissou, D. Copper(I) complexes derived from mono- and diphosphino-boranes: Cu→B interactions supported by arene coordination. *Inorg. Chem.* **2010**, *49*, 3983-3990.

(8)     MacMillan, S. N.; Harman, W. H.; Peters, J. C. Facile Si-H bond activation and hydrosilylation catalysis mediated by a nickel-borane complex. *Chem. Sci.* **2014**, *5*, 590-597.

(9)     Shih, W. C.; Gu, W. X.; MacInnis, M. C.; Timpa, S. D.; Bhuvanesh, N.; Zhou, J.; Ozerov, O. V. Facile insertion of Rh and Ir into a boron-phenyl bond, leading to boryl/bis(phosphine) PBP pincer complexes. *J. Am. Chem. Soc.* **2016**, *138*, 2086-2089.

(10)    Sircoglou, M.; Bouhadir, G.; Saffon, N.; Miqueu, K.; Bourissou, D. A zwitterionic gold(I) complex from an ambiphilic diphosphino-alane ligand. *Organometallics* **2008**, *27*, 1675-1678.

(11)    Sircoglou, M.; Saffon, N.; Miqueu, K.;  Bouhadir, G.; Bourissou, D. Activation of M-Cl bonds with phosphine-alanes: Preparation and characterization of zwitterionic gold and copper complexes. *Organometallics* **2013**, *32*, 6780-6784.

(12)    Semba, K.; Fujii, I.; Nakao, Y. A PAlP pincer ligand bearing a 2-diphenylphosphinophenoxy backbone. *Inorganics* **2019**, *7*, 140.

(13)    For an example of a chelating P-P-Al(alkyl)$_x$ ligand, see: Cowie, B. E.; Tsao, F. A.; Emslie, D. J. H. Synthesis and platinum complexes of an alane-appended 1,1'-bis(phosphino)ferrocene ligand. *Angew*. *Chem*. *Int*. *Ed*. **2015**, *54*, 2165-2169.

(14)    For an example of a more heavily scaffolded PNNNAl(Me)P ligand, see: Saito, T.; Hara, N.; Nakao, Y. Palladium complexes bearing Z-type PAlP pincer ligands. *Chem. Lett.* **2017**, *46*, 1247-1249.

(15)    Miloserdov, F. M.; Isaac, C. J.; Beck, M. L.; Burnage, A. L.; Farmer, J. C. B.; Macgregor, S. A.; Mahon, M. F.; Whittlesey, M. K. Impact of the novel *Z*-acceptor ligand bis{(*ortho*-diphenylphosphino)phenyl}zinc (ZnPhos) on the formation and reactivity of low-coordinate Ru(0) centers. *Inorg. Chem.* **2020**, *59*, 15606-15619.

(16)    Fukuda, K.; Harada, T.; Iwasawa, N.; Takaya, J. Facile synthesis and utilization of bis(o-phosphinophenyl)zinc as isolable PZnP-pincer ligands enabled by boron-zinc double transmetallation. *Dalton Trans.* **2022**, *51*, 7035-7039.

(17)    Isaac, C. J.; Miloserdov, F. M.; Pecharman, A. F.; Lowe, J. P.; McMullin, C. L.; Whittlesey, M. K. Structure and reactivity of [Ru-Al] and [Ru-Sn] heterobimetallic PPh$_3$-based complexes. *Organometallics* **2022**, *41*, 2716-2730.

(18)     Sheldrick, G. M. Crystal structure refinement with SHELXL. *Acta Crystallogr., Sect. C: Struct. Chem.* **2015**, *C71*, 3-8.

(19)     Sheldrick, G. M. SHELXT - Integrated space-group and crystal structure determination. *Acta Crystallogr., Sect. A: Found. Adv.* **2015**, *A71*, 3-8.

(20)     Dolomanov, O. V.; Bourhis, L. J.; Gildea, R. J.; Howard, J. A. K.; Puschmann, H. OLEX2: A complete structure solution, refinement and analysis program. *J. Appl. Crystallogr.* **2009**, *42*, 339-341.

(21)     Frisch, M. J.; Trucks, G. W.; Schlegel, H. B.; Scuseria, G. E.; Robb, M. A.; Cheeseman, J. R.; Scalmani, G.; Barone, V.; Mennucci, B.; Petersson, G. A.; Nakatsuji, H.; Caricato, M.; Li, X.; Hratchian, H. P.; Izmaylov, A. F.; Bloino, J.; Zheng, G.; Sonnenberg, J. L.; Hada, M.; Ehara, M.; Toyota, K.; Fukuda, R.; Hasegawa, J.; Ishida, M.; Nakajima, T.; Honda, Y.; Kitao, O.; Nakai, H.; Vreven, T.; Montgomery, J. A.; Peralta, J. E.; Ogliaro, F.; Bearpark, M.; Heyd, J. J.; Brothers, E.; Kudin, K. N.; Staroverov, V. N.; Keith, T.; Kobayashi, R.; Normand, J.; Raghavachari, K.; Rendell, A.; Burant, J. C.; Iyengar, S. S.; Tomasi, J.; Cossi, M.; Rega, N.; Millam, J. M.; Klene, M.; Knox, J. E.; Cross, J. B.; Bakken, V.; Adamo, C.; Jaramillo, J.; Gomperts, R.; Stratmann, R. E.; Yazyev, O.; Austin, A. J.; Cammi, R.; Pomelli, C.; Ochterski, J. W.; Martin, R. L.; Morokuma, K.; Zakrzewski, V. G.; Voth, G. A.; Salvador, P.; Dannenberg, J. J.; Dapprich, S.; Daniels, A. D.; Farkas, O.; Foresman, J. B.; Ortiz, J. V.; Cioslowski, J.; Fox, D. J. *Gaussian 09,* rev D.01; Gaussian Inc.: Wallingford, CT, 2013.

(22)     Perdew, J. P. Density-functional approximation for the correlation energy of the inhomogeneous electron gas. *Phys. Rev. B: Condens. Matter. Mater. Phys.* **1986**, *33*, 8822-8824.

(23)     Becke, A. D. Density-functional exchange-energy approximation with correct asymptotic behavior. *Phys. Rev. A: At., Mol., Opt. Phys.* **1988**, *38*, 3098-3100.

(24)     Andrae, D.; Häußermann, U.; Dolg, M.; Stoll, H.; Preuß, H. Energy-adjusted ab initio pseudopotentials for the second and third row transition elements. *Theor. Chim. Acta* **1990**, *77*, 123-141.

(25)     Hehre, W. J.; Ditchfield, R.; Pople, J. A. Self-consistent molecular orbital methods. XII. Further extensions of Gaussian-type basis sets for use in molecular orbital studies of organic molecules. *J. Chem. Phys.* **1972**, *56*, 2257-2261.

(26)     Hariharan, P. C.; Pople, J. A. The influence of polarization functions on molecular orbital hydrogenation energies. *Theor. Chim. Acta* **1973**, *28*, 213-222.

(27)     Höllwarth, A.; Böhme, M.; Dapprich, S.; Ehlers, A. W.; Gobbi, A.; Jonas, V.; Köhler, K. F.; Stegmann, R.; Veldkamp, A.; Frenking, G. A set of d-polarization functions for pseudo-potential basis sets of the main group elements Al–Bi and f-type polarization functions for Zn, Cd, Hg. *Chem. Phys. Lett.* **1993**, *208*, 237-240.

(28)     Chai, J.-D.; Head-Gordon, M. Long-range corrected hybrid density functionals with damped atom–atom dispersion corrections. *Phys. Chem. Chem. Phys.* **2008**, *10*, 6615-6620.

(29)     Weigend, F.; Köhn, A.; Hättig, C. Efficient use of the correlation consistent basis sets in resolution of the identity MP2 calculations. *J. Chem. Phys.* **2002**, *116*, 3175-3183.

(30)     Weigend, F. Accurate Coulomb-fitting basis sets for H to Rn. *Phys. Chem. Chem. Phys.* **2006**, *8*, 1057-1065.

(31)     Tomasi, J.; Mennucci, B.; Cammi, R. Quantum mechanical continuum solvation models. *Chem. Rev.* **2005**, *105*, 2999-3094.

(32)     Miloserdov, F. M.; Rajabi, N. A.; Lowe, J. P.; Mahon, M. F.; Macgregor, S. A.; Whittlesey, M. K. Zn-Promoted C-H reductive elimination and $H_2$ activation via a dual unsaturated Ru-Zn intermediate. *J. Am. Chem. Soc.* **2020**, *142*, 6340-6349.

(33)     Bader, R. F. W. *Atoms in Molecules: A Quantum Theory*; Oxford University Press: Oxford, U.K., 1994.

(34)    Keith, T. A. *AIMAll,* ver. 17.11.14, TK Gristmill Software: Overland Park, KS, 2017.

(35)    te Velde, G.; Bickelhaupt, F. M.; Baerends, E. J.; Fonseca Guerra, C.; van Gisbergen, S. J. A.; Snijders, J. G.; Ziegler, T. Chemistry with ADF. *J. Comput. Chem.* **2001**, *22*, 931-967.

(36)    Cordero, B.; Gómez, V.; Platero-Prats, A. E.; Revés, M.; Echeverría, J.; Cremades, E.; Barragán, F.; Alvarez, S. Covalent radii revisited. *Dalton Trans.* **2008**, 2832-2838.

(37)    Dunne, J. P.; Blazina, D.; Aiken, S.; Carteret, H. A.; Duckett, S. B.; Jones, J. A.; Poli, R.; Whitwood, A. C. A combined parahydrogen and theoretical study of $H_2$ activation by 16-electron $d^8$ ruthenium(0) complexes and their subsequent catalytic behaviour. *Dalton Trans.* **2004**, 3616-3628.

(38)    Neither changing $H_2$ to $Me_2NH.BH_3$, nor $C_6H_6$ to THF, produced $[Ru(PPh_3)_2(CO)_2H_2]$-free **2**.

(39)    During the preparation of **2-$^{13}$CO** by photolysis of **1-$^{13}$CO** under $H_2$, we also observed the formation of a second by-product, which was identified by $^{31}$P and $^{13}$C NMR spectroscopy as $[Ru(PPh_3)_2(^{13}CO)_3]$ (Kubis, C.; Profir, I.; Fleischer, I.; Baumann, W.; Selent, D.; Fischer, C.; Spannenberg, A.; Ludwig, R.; Hess, D.; Franke, R.; Borner, A. In-situ FTIR and NMR spectroscopic investigations on ruthenium-based catalysts for alkene hydroformylation. *Chem. Eur. J.* **2016**, *22*, 2746-2757). This forms through the thermal reaction of $[Ru(PPh_3)_2(CO)_2H_2]$ with the photoeliminated CO (Jessop, P. G.; Rastar, G.; James, B. R. Substitution reaction mechanisms of dihydrido-ruthenium(II) phosphine complexes: Hydride basicity and molecular hydrogen intermediates. *Inorg. Chim. Acta* **1996**, *250*, 351-357). Thus any attempt to prepare **2** on a large scale, which would necessitate prolonged irradiation, would be plagued by the formation of $[Ru(PPh_3)_2(CO)_2H_2]$, as well as the Ru(0) tricarbonyl complex.

(40)    We have measured a $T_1$ value (400 MHz, 298 K) of 1.27 s for [Ru(ZnPhos)(CO)$_2$(μ-H)$_2$] (**3**, Scheme 2).

(41)    Coles, M. P.; Jordan, R. F. Cationic aluminum alkyl complexes incorporating amidinate ligands. Transition-metal-free ethylene polymerization catalysts. *J. Am. Chem. Soc.* **1997**, *119*, 8125-8126.

(42)    Stanga, O.; Lund, C. L.; Liang, H.; Quail, J. W.; Müller, J. Synthesis and characterization of neutral and cationic intramolecularly coordinated aluminum compounds. Structural determination of [(Pytsi)AlMe]$^+$[MeB(C$_6$F$_5$)$_3$]$^-$ [(Pytsi = C(SiMe$_3$)$_2$SiMe$_2$(2-C$_5$H$_4$N)]. *Organometallics* **2005**, *24*, 6120-6125.

(43)    Horton, A. D. Direct observation of β-methyl elimination in cationic neopentyl complexes: Ligand effects on the reversible elimination of isobutene. *Organometallics* **1996**, *15*, 2675-2677.

(44)    Ciancaleoni, G.; Fraldi, N.; Budzelaar, P. H. M.; Busico, V.; Macchioni, A. Activation of a bis(phenoxy-amine) precatalyst for olefin polymerisation: First evidence for an outer sphere ion pair with the methylborate counterion. *Dalton Trans.* **2009**, 8824-8827.

(45)    Kim, K. C.; Reed, C. A.; Long, G. S.; Sen, A. Et$_2$Al$^+$ alumenium ion-like chemistry. Synthesis and reactivity toward alkenes and alkene oxides. *J. Am. Chem. Soc.* **2002**, *124*, 7662-7663.

(46)    Engesser, T. A.; Lichtenthaler, M. R.; Schleep, M.; Krossing, I. Reactive p-block cations stabilized by weakly coordinating anions. *Chem. Soc. Rev.* **2016**, *45*, 789-899.

(47)    Franz, D.; Inoue, S. Cationic complexes of boron and aluminium: An early 21$^{st}$ century viewpoint. *Chem. Eur. J.* **2019**, *25*, 2898-2926.

(48)    Dagorne, S.; Bellemin-Laponnaz, S.; Welter, R. Synthesis and structure of neutral and cationic aluminum complexes incorporating bis(oxazolinato) ligands. *Organometallics* **2004**, *23*, 3053-3061.

(49)    Miloserdov, F. M.; Pécharman, A.-F.; Sotorrios, L.; Rajabi, N. A.; Lowe, J. P.; Macgregor, S. A.; Mahon, M. F.; Whittlesey, M. K. Bonding and reactivity of a pair of neutral and cationic heterobimetallic RuZn$_2$ complexes. *Inorg. Chem.* **2021,** *60*, 16256-16265.

(50)    Lepetit, C.; Fau, P.; Fajerwerg, K.; Kahn, M. L.; Silvi, B. Topological analysis of the metal-metal bond: A tutorial review. *Coord. Chem. Rev.* **2017**, *345*, 150-181.

(51)    Adams, G. M.; Weller, A. S. POP-type ligands: Variable coordination and hemilabile behaviour. *Coord. Chem. Rev.* **2018**, *355*, 150-172.

**ToC Graphic and Text**

A combination of experimental and computational approaches show that the Lewis acidities of the novel *Z*-acceptor pincer phosphine ligands (*o*-Ph$_2$PC$_6$H$_4$)$_2$AlMe (AlMePhos) and [(*o*-Ph$_2$PC$_6$H$_4$)$_2$Al]$^+$ (AlPhos) in [Ru(AlMePhos)(CO)$_3$] and [Ru(AlPhos)(CO)$_3$]$^+$ respectively are greater than those of the previously reported Zn-analogue (*o*-Ph$_2$PC$_6$H$_4$)$_2$Zn (ZnPhos).